A HOLISTIC APPROACH TO FLUTTER CLEARANCE USING CLASSICAL METHODS

Louw H van Zyl*
***CSIR, South Africa**

Keywords: *flutter analysis, flutter flight testing, state-space model*

Abstract

Flutter clearance is usually regarded as a two-step process: flutter analysis (including ground vibration testing, aerodynamic analysis and equation of motion solution), and flutter flight testing. The problem with this approach is that there are often significant discrepancies between the predicted damping and frequency trends and the trends measured during flutter flight testing. The discrepancies, when they become apparent during flight testing, cast doubt on the accuracy and validity of the analysis and hamper processing of the flight test data. By employing relatively simple techniques in combination, the analyst can be much better prepared for the flutter flight tests, enabling him to process the data efficiently despite the usual discrepancies and to better judge whether the discrepancies indicate serious deficiencies in the flutter analysis.

1 Introduction

It is not unusual to find significant discrepancies between flutter analysis results and flutter flight test results for general aviation aircraft. The discrepancies can be attributed to measurement errors during the ground vibration test, modal truncation, deficiencies in aerodynamic modeling, differences between the ground vibration test aircraft and the flight test aircraft, differences between actual and assumed fuel states, finite frequency resolution in flight test data, assumptions made in determining damping and frequency from flight test data, and measurement noise during flight tests. An approach is suggested to minimize the uncertainty and sometimes confusion caused by these discrepancies.

The key technique is to generate a state-space model from the frequency domain flutter analysis matrices. The model is validated by determining and eigenvalue solution from the state-space model and comparing it to the frequency domain solution. This model is then used to generate time histories of the responses of the different sensors that will be used in flutter flight testing for a given excitation configuration. The time histories are processed by the flutter flight test software to assess how well the vibration modes are excited and to determine the effect of the finite frequency resolution and the assumptions made in the data processing on the modal parameters. The best excitation parameters (position, sweep duration and frequency limits) and the most suitable data processing techniques can also be established.

The process is illustrated in the Fig. 1. The ground vibration test (GVT) typically consists of a Phase Separation test, followed by a Phase Resonance test to obtain better modal parameters for a number of modes if it is deemed necessary. The unsteady aerodynamic analysis for a business jet class of aircraft would make use of the standard doublet lattice method (DLM) of Rodden et al. [1] or the transonic doublet lattice method (TDLM) of Lu and Voβ [2]. The TDLM requires the steady pressure distribution in the flow field around the wings as input and modifies the downwash matrix accordingly in order to obtain a reasonable unsteady transonic pressure distribution.

The minimum-state approximation uses the method of Karpel [3] with lag root optimization [4], yielding the best accuracy for a given number of lag roots. The time-domain simulation is relatively straightforward and is done using the modal basis. The excitation forces are generalized by the modal displacements at the point of application of the forces. The responses at the sensor locations are similarly determined from the modal basis solution and the modal displacements at the sensors.

The flutter flight test software processes the time histories to power spectral density plots (PSDs). The PSD for each channel is displayed to the user, who must select the peaks that are clear enough to extract frequency and damping estimates. The user must also assign each selected peak to a vibration mode. Since it is essential to assign PSD peaks to modes consistently in order to have valid results, the software incorporates presentations of the data that would make any inconsistencies apparent.

2 Application

The example chosen to illustrate the process is that of a light aerobatic aircraft, shown in Fig. 2. The aircraft was developed to compete in the advanced world aerobatic class and the layout is based on the popular Laser aircraft. The construction is full composite and the control surfaces are of a new design, therefore it was treated as a new design for flutter clearance purposes. Aircraft of this type are generally light and stiff, making flutter of the primary structure unlikely. However, in order to achieve competitive performance, control surfaces are under-balanced as much as possible to reduce the aircraft overall inertia and the control system inertia.

2.1 Ground Vibration Test

A phase separation test was performed first, after which all the identified modes were extracted using a phase resonance technique. The following modes were extracted:

Table 1: Symmetric modes

Mode	Frequency [Hz]	Mass [kg]	Description
1	12.47	21.5	First wing bending
6	21.21	144.6	Second wing bending
7	24.80	126.2	First wing torsion
11	36.24	17.2	Stabiliser bending

Table 2: Anti-symmetric modes

Mode	Frequency [Hz]	Mass [kg]	Description
2	14.15	65.4	Fuselage torsion
3	15.56	17.7	Stabiliser roll
4	17.31	37.4	Stabiliser roll, fin bending out of phase
5	21.12	20.8	Fin bending, stabiliser roll out of phase
8	25.63	33.5	First wing bending

Table 3: A-symmetric modes

Mode	Frequency [Hz]	Mass [kg]	Description
9	30.59	12.5	Right wing torsion
10	28.36	18.9	Left wing torsion

To this list was added the control surface modes. Control surfaces do not have a natural frequency unless the system contains centring springs. Only the modal mass of each control mode (aileron deflection, rudder deflection and elevator deflection) was determined experimentally. In flight, the airflow over the control surfaces provides a restoring force that acts like a spring, and the control surface modes have frequencies that increase with increasing speed.

Table 4: Control surface modes

Mode	Control mode	Position of unit displacement	Modal mass [kg]
12	Elevator	Inboard trailing edge	2.0
13	Aileron	Inboard trailing edge	3.0
14	Rudder	510 mm aft of hinge line	1.6

A typical the micro-scan result from which the modal parameters are determined is shown in Fig. 3 and a graphical presentation of a mode shape is shown in Fig. 4.

2.2 Flutter analysis

The DLM was used to generate the generalized forces for the modes listed above, and the p-k formulation of the flutter equation [5] was solved to obtain the frequency and damping of each mode as a function of air speed. The modal mass matrix was modified to take account of the changes in control surface mass balancing between the GVT and flight tests, and the mass of the wing tip-mounted excitation system. The typical frequency and damping vs air speed plots are shown in Fig. 5 and Fig. 6.

2.3 State-space model

The minimum-state method of Karpel was used with lag root optimization to produce a state-space model for the configuration. Ten lag rots were used and the model was verified by determining the frequency and damping as a function of air speed from the eigenvalues of the state-space system matrix. These results are shown in Fig. 7 and Fig. 8. The correlation with the p-k solution was deemed satisfactory.

2.4 Time domain solution

Time domain solutions were generated from the state-space model at several speeds over the expected flight test speed range. The excitation was applied at the position of the wings of the wing tip excitation system. Symmetric and anti-symmetric excitation was applied at each speed. Accelerations were determined at the six locations that were used in the flight tests. Tables of the displacement of the force application points and the response measurement points were used to generalize the excitation forces and to extract physical responses from the modal basis solution.

The sensitivities of the strain gauges and accelerometers were applied and the output of the simulation was presented with a resolution similar to the A/D converters used in the flight tests. The offsets due to the accelerometer orientation (the type used measures steady acceleration) were also added. This was done to obtain an indication of possible saturation of the sensors or low response levels.

The calculated time histories of the wing-mounted accelerometer outputs at 200 KEAS are shown in Fig. 9. A good response level without saturation is indicated.

The actual time histories measured during the flight test are shown in Fig. 10. The engine-induced vibration level was high due to the powerful engine, stiff engine mounts and light, stiff structure that is typical of this class of aircraft. The additional vibration caused some saturation which was not predicted by the simulation.

2.5 Flight test software results

The flight test software that was used calculates the PSD of each input channel. This is displayed to the user who selects significant peaks. The selected peaks are automatically assigned to modes based on the frequency of the selected peak and the predicted modal frequencies at that speed. The user can override the assignment of individual peaks and also manually change the predicted frequencies used by the automatic mode assignment algorithm.

The flutter flight test software can read in simulated time histories and process it in exactly the same way as actual flight test data. This gives an indication of which modes will be excited and sensed effectively, and to what extent close spacing of modes will affect the extraction of damping values.

PSDs generated by the flight test software for the wing-mounted accelerometers are shown in Fig. 11. The PSDs of the corresponding measured outputs are shown in Fig. 12. The simulation correctly predicts the relative amplitudes of modes 1 and 7 on the two outputs. There is a glaring discrepancy in that the

simulation predicts that mode 10 would be well excited and measured, whereas it does not pear in the actual flight test data. The PSDs of the excitation forces shown in Fig. 13 reveal that there was very little actual excitation above 28 Hz, whereas the simulation assumed constant force levels up to 40 Hz. It is not known whether the excitation system did not turn at the specified 40 Hz or whether the drop in excitation force was due to flexibility in the installation.

Fig. 14 and Fig. 15 show some comparisons between predicted frequency and damping results and frequency and damping values calculated by the flutter flight test software. The results using simulated data indicate that the frequency resolution and processing method could be expected to give accurate results.

3 Conclusions

A procedure has been proposed to reduce or at least understand the differences between flutter analysis and flutter flight test results. It is applicable to most instances where aero-elastic considerations are not an integral part of the design process, typically homebuilt projects, new general aviation aircraft and small business jets. Application of the procedure to the flutter clearance of an aerobatic aircraft proved the value of the simulation in the planning of a flight test as well as interpreting the data.

References

[1] Rodden, W. P., Taylor, P. F. and McIntosh, S. C., Jr. Further refinement of the nonplanar aspects of the subsonic doublet-lattice lifting surface method. *Proc 20th Congress of the International Council of the Aeronautical Sciences*, Sorrento, Italy, Vol. 2, paper 96-2.8.2, pp 1786-1799, 1996.

[2] Lu, S., and Voβ, R.. *TDLM – A transonic doublet lattice method for 3D unsteady potential flow calculation*. DLR Institut für Aeroelastik, Göttingen, Germany, DLR-FB 92-25, 1992.

[3] Karpel, M., and Tiffany, S. H. *Physically Weighted Approximations of Unsteady Aerodynamics Forces Using the Minimum-State Method*. NASA TP-3025, March 1991.

[4] Van Zyl, L.H. Optimisation of aerodynamic lag roots in minimum-state approximations. *Proc International Forum on Aeroelasticity and Structural Dynamics 2003*, Amsterdam, The Netherlands.

[5] Rodden, W.P., Harder, R.L., and Bellinger, E.D. *Aeroelastic Addition to NASTRAN*. NASA CR 3094, March 1979.

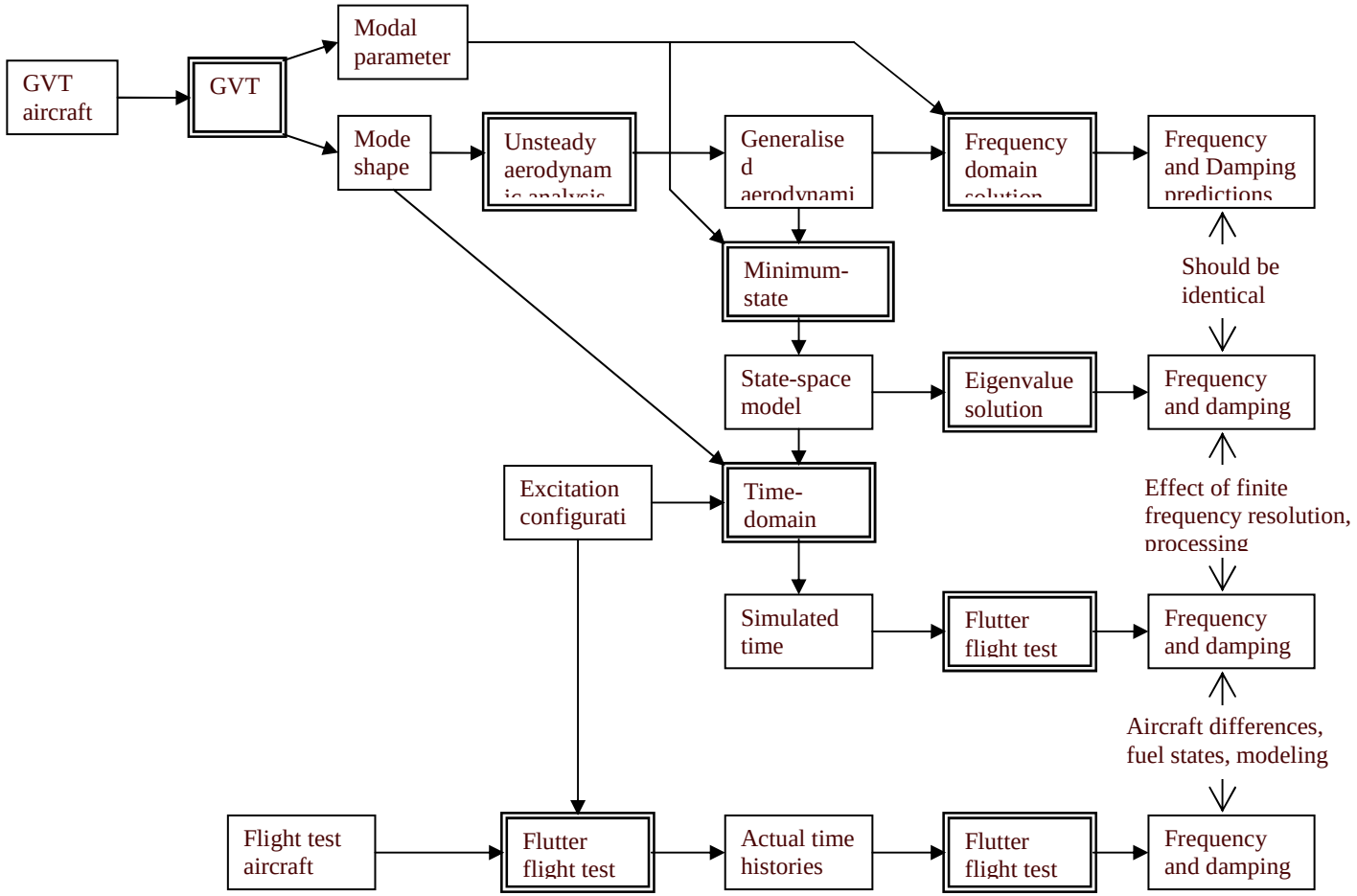

Fig. 1: Proposed flutter clearance process

Fig. 2: The Slick 360 aerobatic aircraft

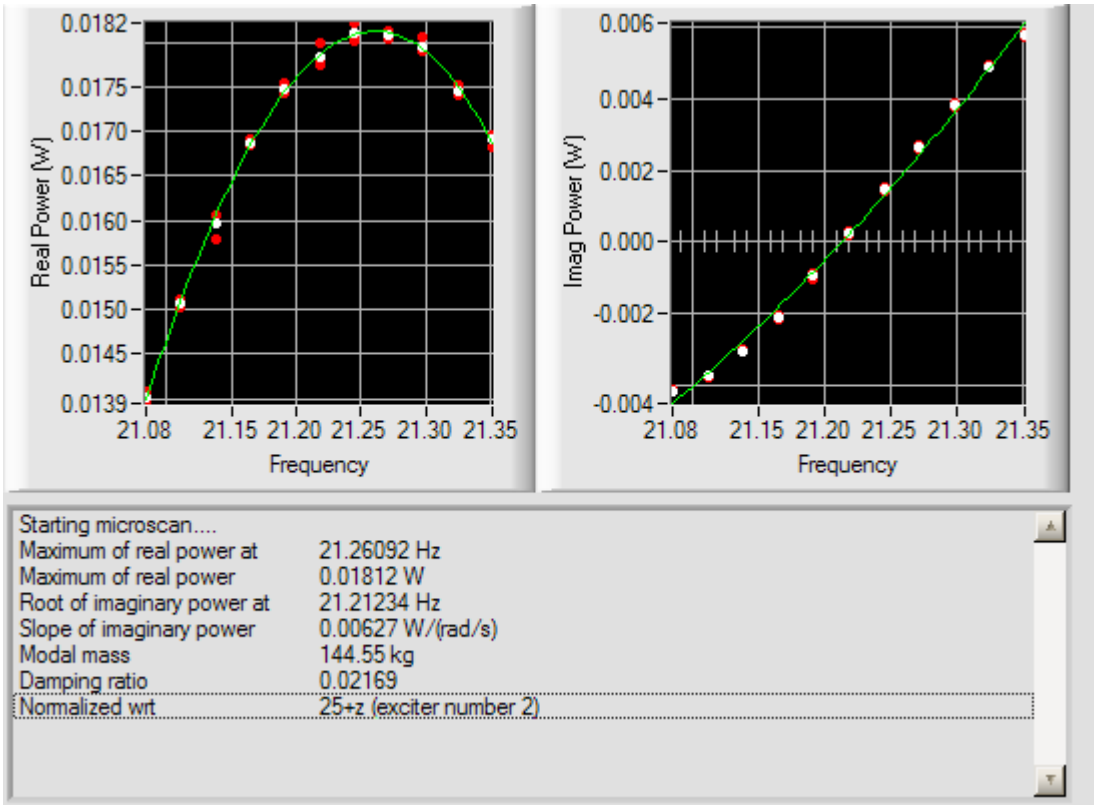

Fig. 3: Modal parameter extraction for the second symmetric wing bending mode

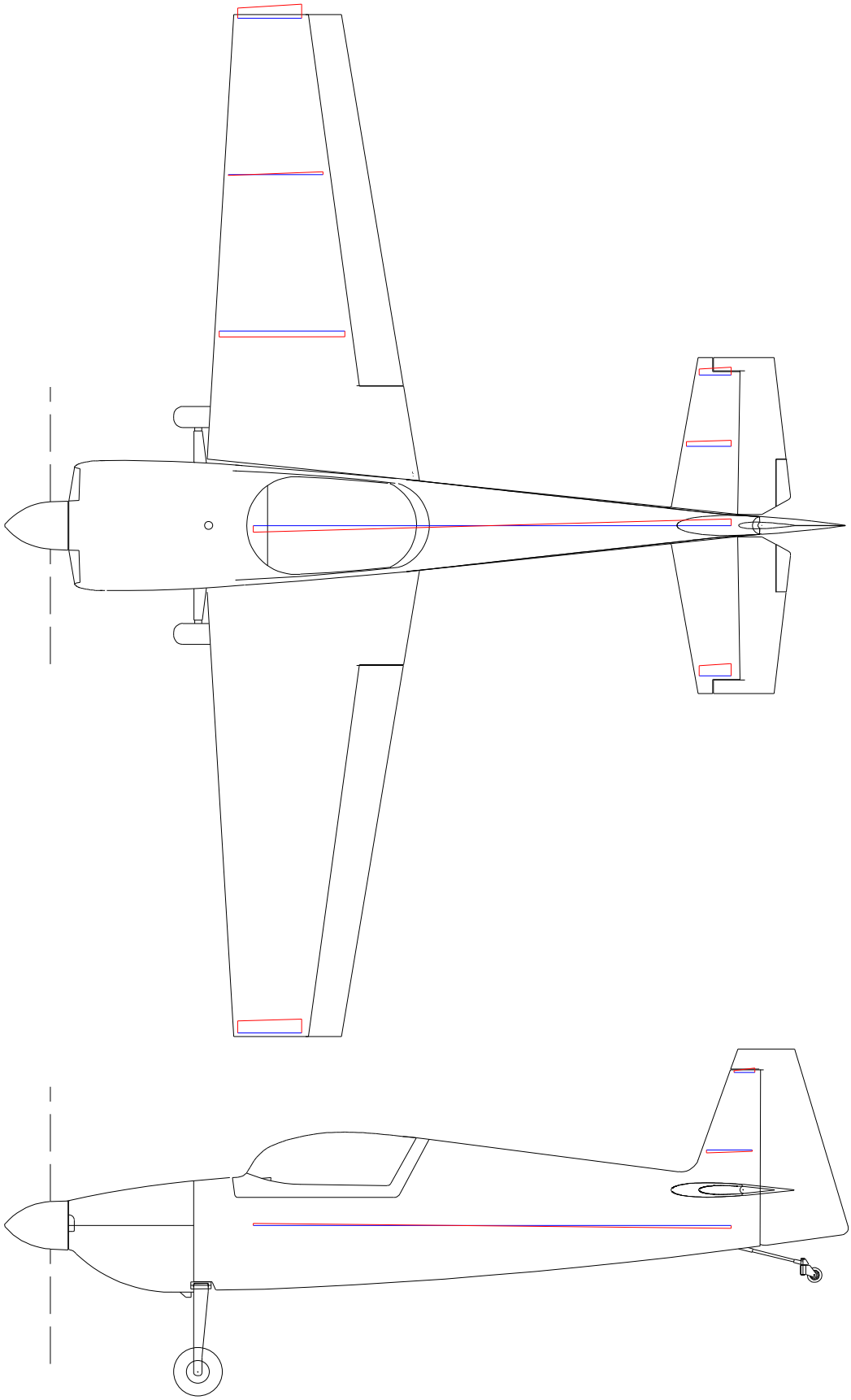

Fig. 4: Second symmetric wing bending mode

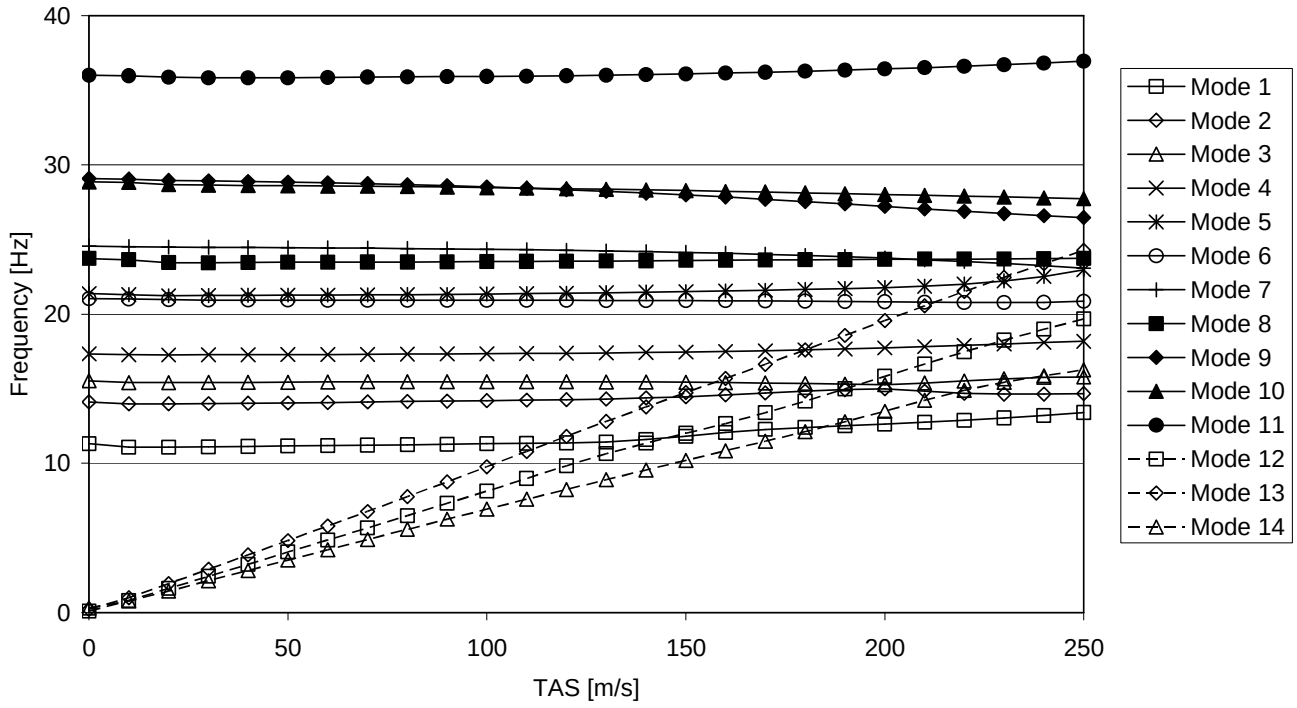

Fig. 5: Frequency vs air speed from p-k flutter analysis

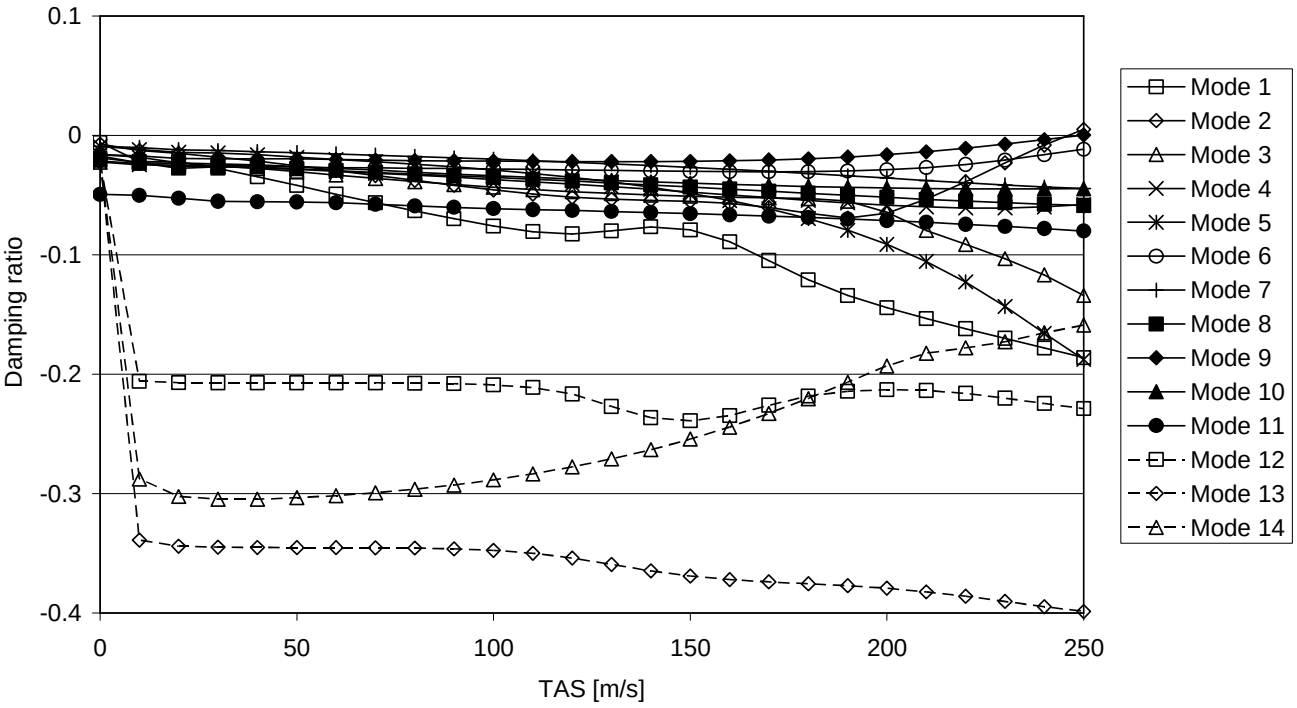

Fig. 6: Damping vs air speed from p-k flutter analysis

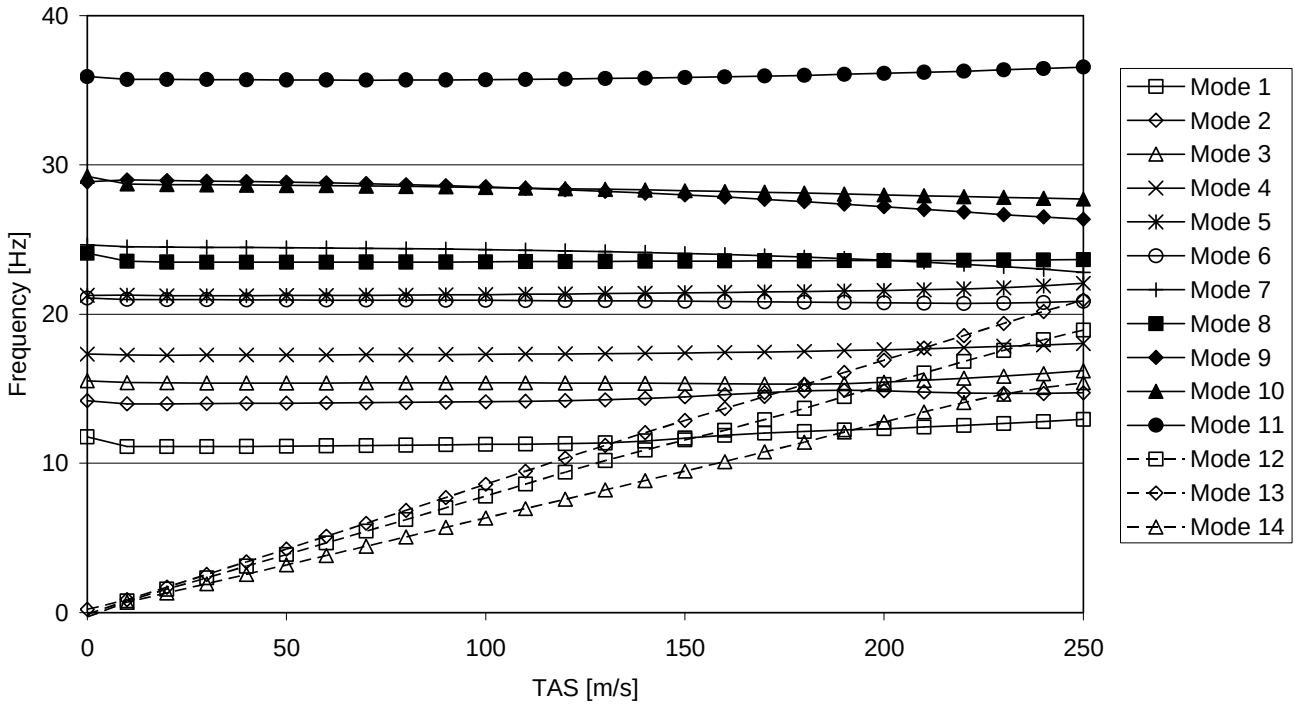

Fig. 7: Frequency vs air speed from state-space model eigenvalue solution

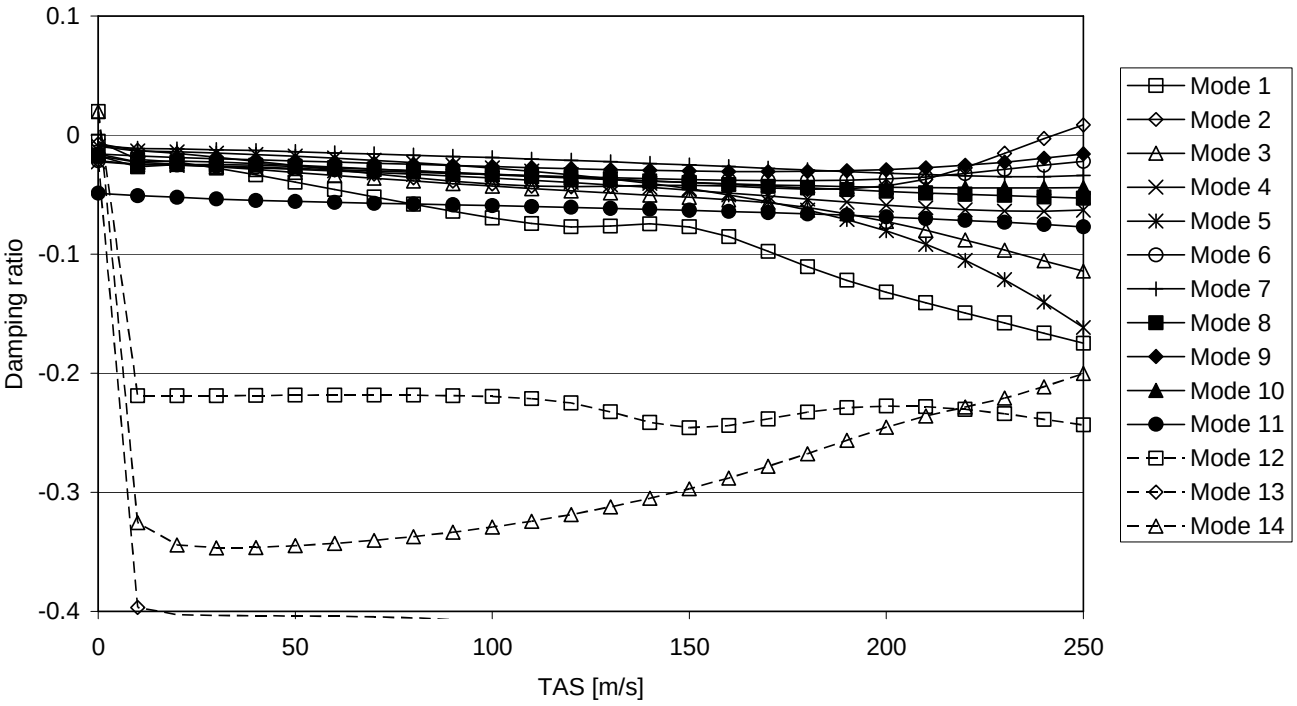

Fig. 8: Damping vs air speed from state-space model eigenvalue solution

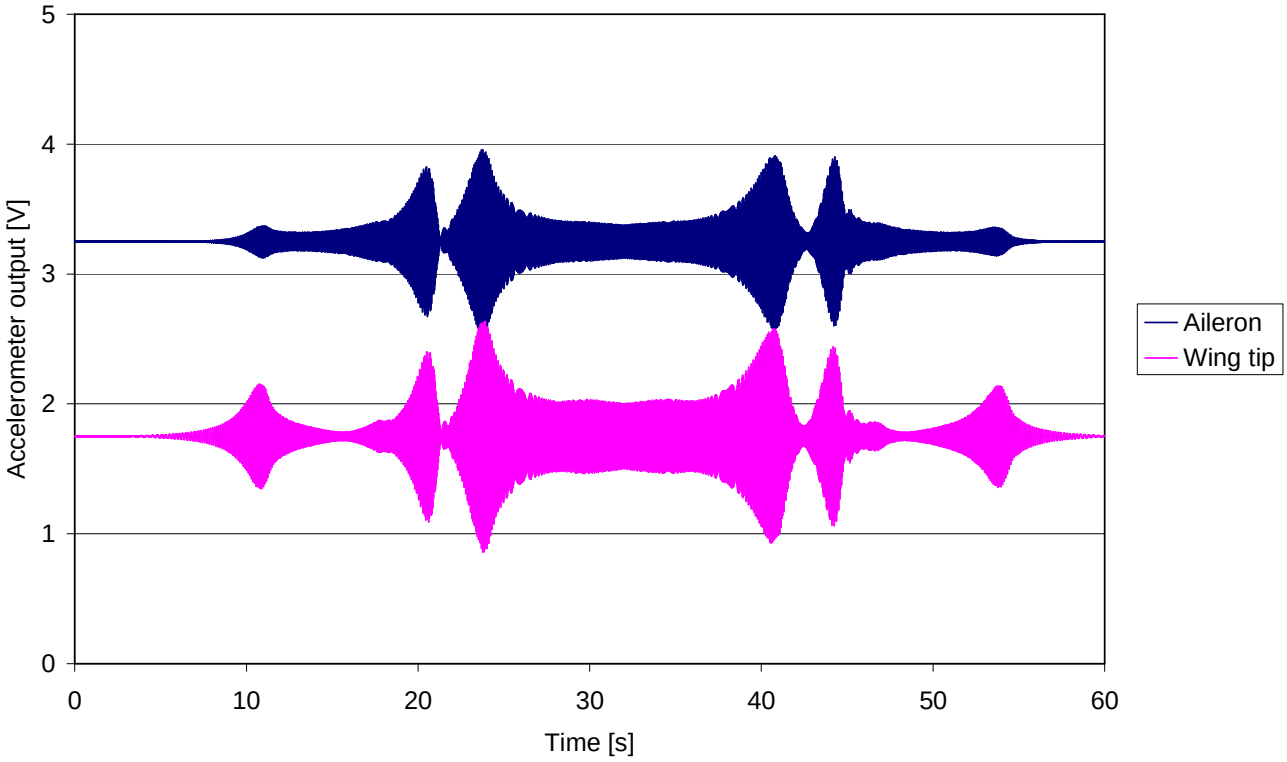

Fig. 9: Calculated wing-mounted accelerometer output at 200 KEAS

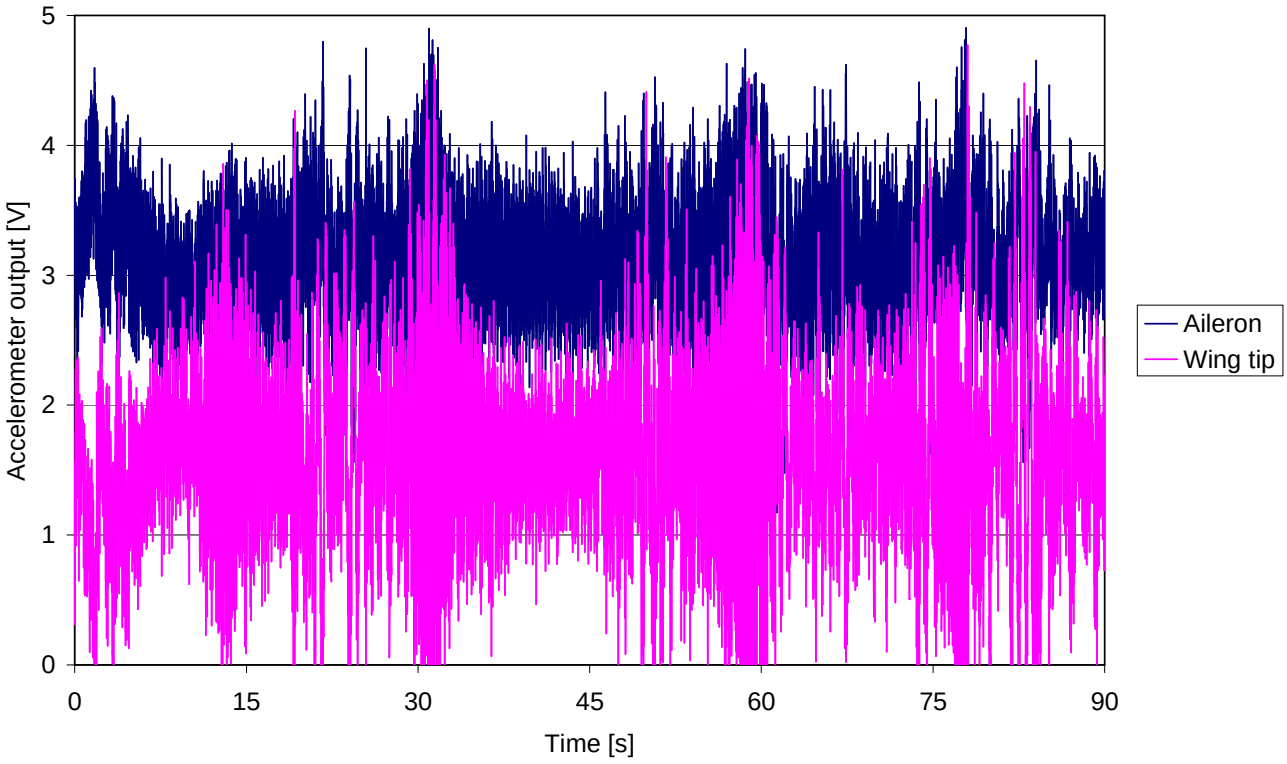

Fig. 10: Measured wing-mounted accelerometer output at 200 KEAS

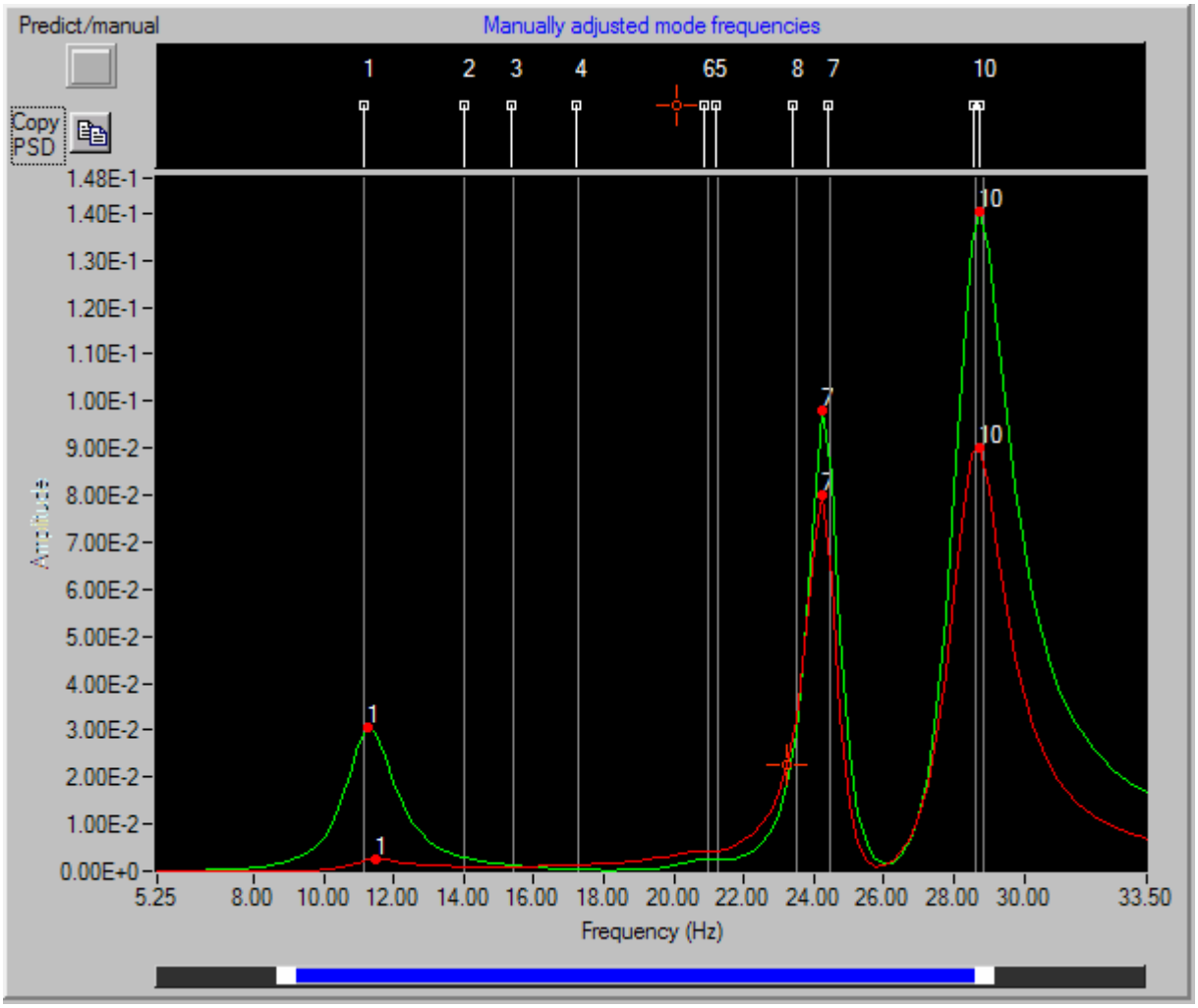

Fig. 11: PSDs of calculated aileron-mounted (red) and wing tip-mounted (green) accelerometer output at 200 KEAS

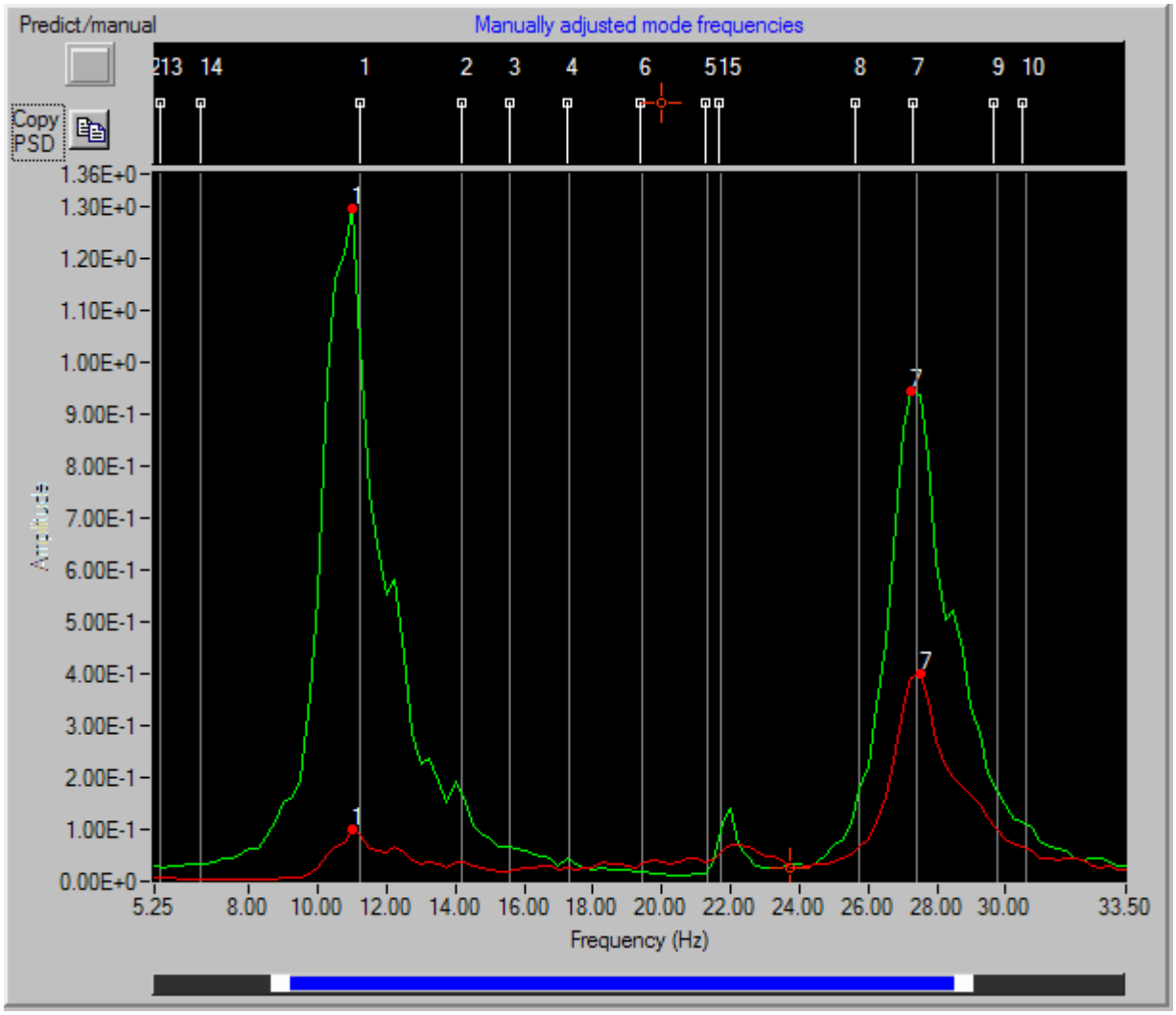

Fig. 12: PSDs of measured aileron-mounted (red) and wing tip-mounted (green) accelerometer output at 200 KEAS

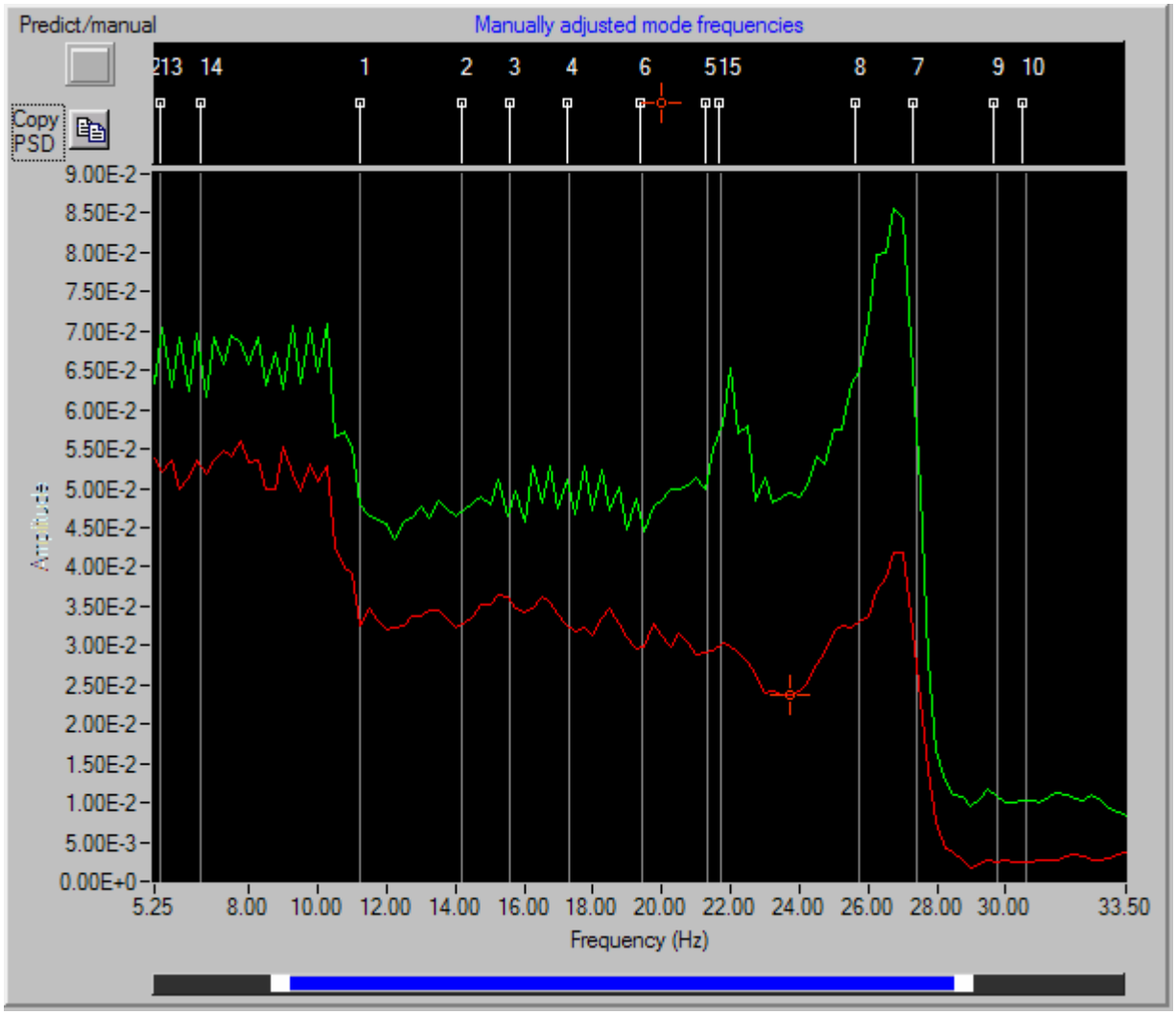

Fig. 13: PSDs of excitation forces

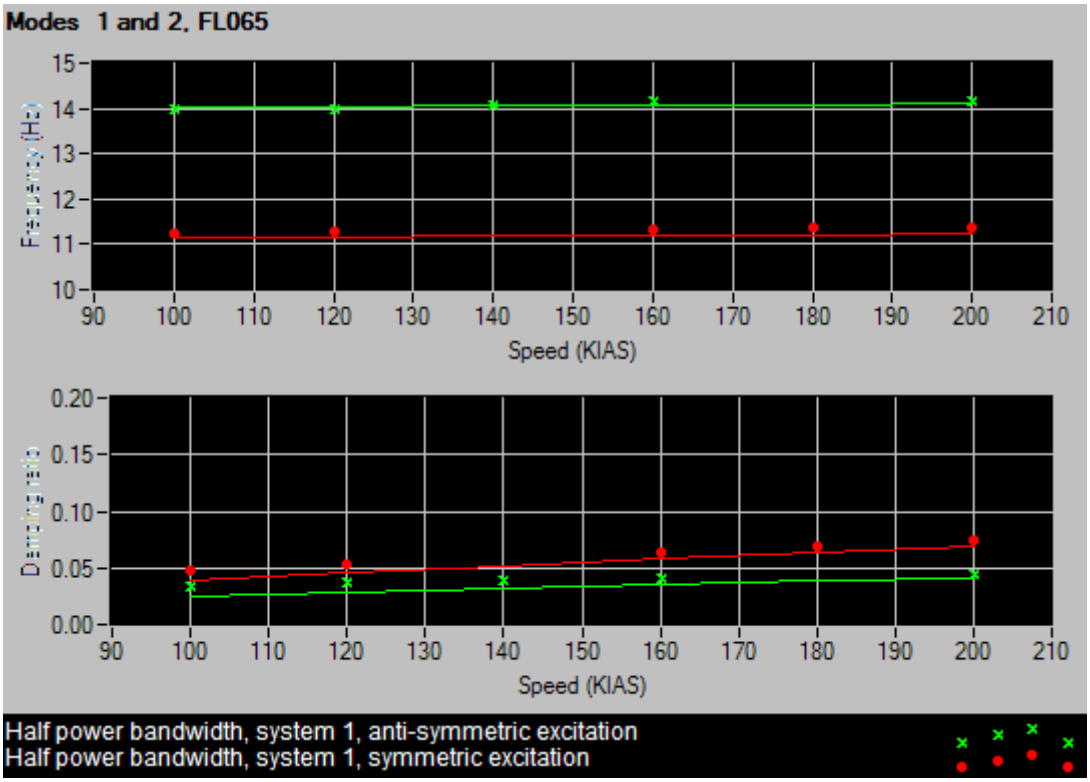

Fig. 14: Comparison between eigenvalue solution and simulated flight test results, modes 1 and 2

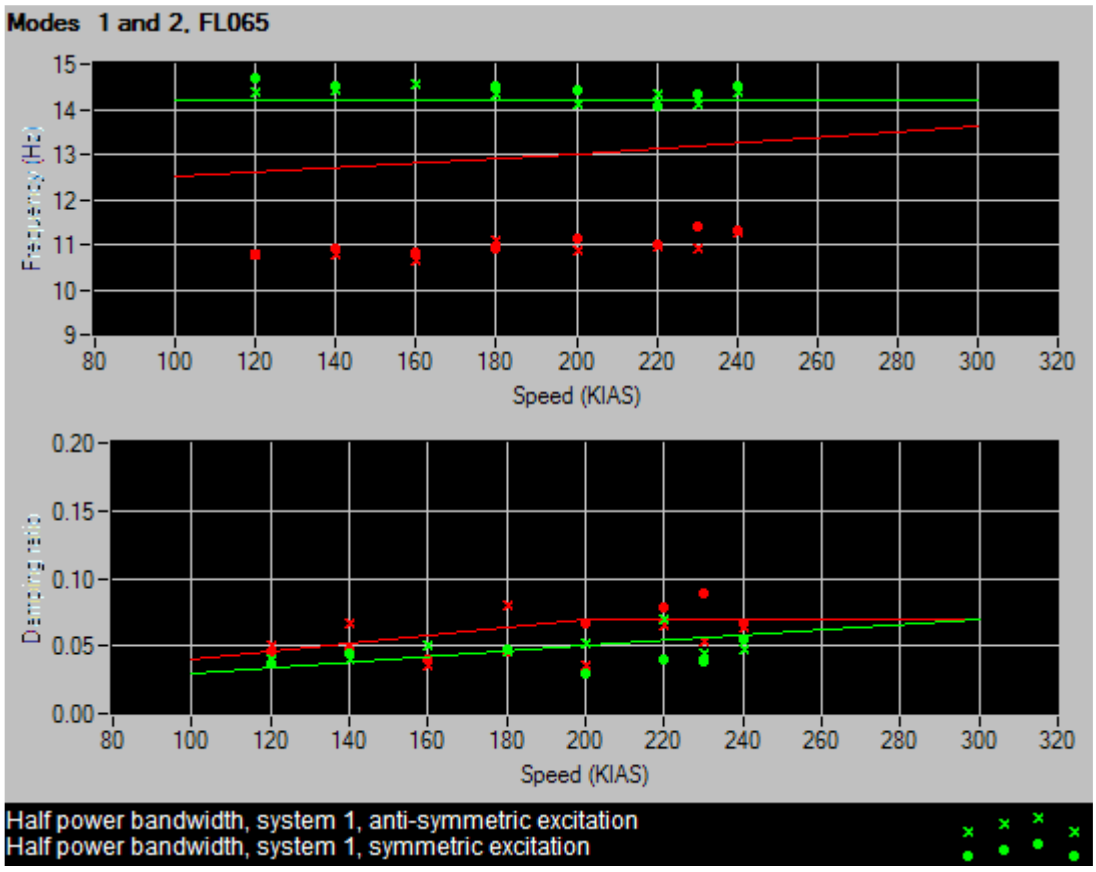

Fig. 15: Comparison between p-k flutter analysis and flight test results, modes 1 and 2